Ecological Indicators 169 (2024) 112819

Contents lists available at ScienceDirect

Ecological Indicators

journal homepage: www.elsevier.com/locate/ecolind

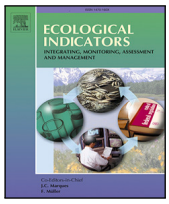

Original articles

Invasion of Pine Wilt Disease: A threat to forest carbon storage in China

Bohai Hu [a,b], Wenjiang Huang [a,b,*], Zhuoqing Hao [a,b], Jing Guo [a,b], Yanru Huang [a,b], Xiangzhe Cheng [a,b], Jing Zhao [a], Quanjun Jiao [a], Biyao Zhang [a]

[a] State Key Laboratory of Remote Sensing Science, Aerospace Information Research Institute, Chinese Academy of Sciences, Beijing 100094, China
[b] University of Chinese Academy of Sciences, Beijing 100049, China

ARTICLE INFO

Keywords:
Pine wilt disease
Remote sensing
Forest carbon storage
Carbon loss
Carbon recovery

ABSTRACT

China's forests, which balance atmospheric carbon (C) levels through photosynthesis, play a crucial role in combating global climate change. The emergence of Pine wilt disease (PWD), caused by the pine wood nematode (PWN, *Bursaphelenchus xylophilus*), has challenged the stability of these forests, leading to significant tree mortality and disrupting the original ecological balance. However, the impact of PWD on carbon storage and recovery in Chinese forests remains unclear. In this study, we integrated multiple data sources, including forest surveys, remote sensing, and meteorological observations, and applied a method of finely partitioning the resistance of host pine trees across China. Using the MaxEnt model, a live carbon risk model, and a C recovery REGIME model that incorporates disturbance mechanisms, we predicted the forest C risk loss caused by the comprehensive invasion of PWD and assessed the C recovery time for affected forests. We estimate that the total risk of C loss due to PWD invasion under current climate conditions in Chinese forests is 483.23 Tg C, with an average C recovery time of 13.95 years. The main risk areas for PWD are concentrated in the southern coastal regions of China and adjacent provinces, presenting a risk spillover pattern that radiates from focal areas outward. The six provinces with the highest forest risk degree (risk C/total regional C) are, in order, Fujian (13.69%), Zhejiang (9.42%), Hunan (7.49%), Guangxi (7.40%), Jiangxi (7.35%), and Guangdong (7.05%). Our findings indicate that the severe consequences of PWD invasion have transformed affected forests from C sinks to sources. This underscores the urgency of implementing effective measures to block its introduction and spread, thereby promoting the recovery and sustainable development of forest ecosystems.

1. Introduction

China's forest ecosystems, spanning vast geographical areas, constitute a crucial component of the global carbon cycle (Ji et al., 2020). In the fight against global climate change, these forests play a vital role (Nunes et al., 2020), acting as vast carbon sinks. Through photosynthesis, they balance atmospheric carbon levels, maintaining ecological equilibrium and playing a crucial role in reducing greenhouse gas concentrations (Collalti et al., 2020). Despite the significant contribution of China's forests to the global carbon balance, their carbon storage capacity is not unshakeable. The onset of Pine Wilt Disease (PWD), induced by the pine wood nematode (PWN, Bursaphelenchus xylophilus), significantly undermines this stability (Gao et al., 2018). As an invasive disease, PWD, spread by insects like the sawyer beetle, has been proliferating in China since the 1980s (Liu et al., 2021), becoming a leading cause of death for pine trees in China's coniferous forests (Mamiya, 1983). Research indicates that in 2020 alone, it affected over 1.81 million hectares of forests, leading to the death of approximately 19.5 million pine trees (Wang et al., 2022). After PWD-induced tree mortality, the needles of pine trees rapidly change from green to red (Mitchell and Preisler, 1998), and photosynthesis ceases, leading to a decrease in the forest's net primary productivity (NPP) (Brown et al., 2010; Pfeifer et al., 2011). Simultaneously, the dead trees fall, and the litter undergoes decomposition, or the infected trees are actively burned, resulting in an increase in heterotrophic respiration (Edburg et al., 2011). In severe outbreaks, the combined effects of reduced NPP and increased heterotrophic respiration can cause the forest to shift from a carbon sink to a carbon source, as large-scale tree mortality due to pest outbreaks directly impacts the forest's carbon storage capacity (Kurz et al., 2008). Furthermore, the ecological disturbances caused by PWD are highly sensitive to climate change, and the resultant carbon loss could exacerbate the feedback mechanisms driving climate change (Thom et al., 2017). Therefore, it is imperative to conduct in-depth research and assess the long-term impact of PWD on forest carbon storage, which is essential not only for

* Corresponding author at: State Key Laboratory of Remote Sensing Science, Aerospace Information Research Institute, Chinese Academy of Sciences, Beijing 100094, China.
E-mail address: huangwj@aircas.ac.cn (W. Huang).

https://doi.org/10.1016/j.ecolind.2024.112819
Received 6 July 2024; Received in revised form 8 October 2024; Accepted 4 November 2024
Available online 14 November 2024

accurately predicting and quantifying the potential of forests as carbon sinks but also for devising effective forest management strategies to preserve their ecosystem services.

Traditional studies on forest carbon loss due to pest outbreaks typically rely on forest inventory data, combined with modeling to assess biomass reductions caused by host tree mortality, thereby estimating carbon loss (Foster, 2011; Liu et al., 2011). One notable example is the cumulative assessment of the mountain pine beetle (*Dendroctonus ponderosae Hopkins*) outbreak in British Columbia, Canada, from 2000 to 2020, which revealed a carbon loss of up to 270 million tons (Mt), equivalent to 75% of the annual direct forest fire emissions in Canada between 1959 and 1999 (Kurz et al., 2008). Similarly, data from the U.S. Forest Inventory and Analysis (FIA) program quantified the effects of insect and disease disturbances on forest carbon sequestration, showing a reduction in carbon accumulation by 69% in insect-affected plots and 28% in disease-affected plots, leading to an annual carbon loss of approximately 12.83 Tg (Quirion et al., 2021). These findings underscore the significant impact of pest outbreaks on forest carbon storage, where diminished carbon sequestration and increased biomass carbon release also elevate natural disaster risks. The black pine beetle outbreak, for example, heightened fire risks while accelerating carbon loss through rapid biomass decay (Hunt et al., 2006). In Europe, reductions in oak populations due to biotypic pest outbreaks further disrupted the carbon–nitrogen cycle, altering the long-term carbon storage capacity of forest ecosystems (lM Arnold et al., 2016). These field studies and modeling simulations provide essential insights into the impact of pest outbreaks on forest carbon pools, forming a solid foundation for quantitative assessments of carbon loss.

With the continuous advancement of drone and satellite remote sensing technologies, methods that utilize instantaneous or short-term imagery to capture carbon losses in affected areas have gradually replaced traditional on-site forest surveys (Shaikh et al., 2022). These studies primarily focus on directly observing carbon losses in already infected regions. By integrating remote sensing data with field observations, researchers can more accurately assess biomass changes in affected areas and estimate the corresponding carbon stock losses (Goetz and Dubayah, 2011; Bustamante et al., 2016). For instance, the combination of field observations, drone-based LIDAR data, and multispectral imagery has been employed to quantify the impact of pine beetle infestations on above-ground carbon stocks in North America (Bright et al., 2012). This approach highlights the effectiveness of using instantaneous remote sensing data to evaluate large-scale pest outbreaks. Additionally, high-resolution satellite imagery from WorldView-2 has been utilized to estimate carbon losses caused by the Sal heartwood borer (*Hoplocerambyx spinicomii*) (Valley, 2014). By merging remote sensing imagery with above-ground biomass data, their study calculated the average carbon stock in the study area to be 108 Mg C/ha and simulated risk areas based on factors such as proximity to villages, humidity, and tree diameter. Although these static studies are powerful tools for assessing immediate carbon losses, they are limited in their ability to identify future potential risk areas.

To address the limitations of static remote sensing imagery in assessing carbon losses, researchers have increasingly incorporated species distribution models (SDMs) into pest-related carbon loss assessments in recent years. By integrating remote sensing data with SDM models, it becomes possible to not only identify current carbon loss but also predict potential high-risk areas for future losses. MaxEnt, with its flexibility in handling multiple variables and its ability to adapt to sparse data, has emerged as a leading tool in this field (Zhang et al., 2021; Yuan et al., 2015). A study that combined principal component analysis (PCA) and MaxEnt mapped the potential impact of pine wilt disease (PWD) on forest carbon stocks in northeastern China, projecting an increase of approximately 39,000 square kilometers in carbon stock loss by 2061–2100 (Wang et al., 2023). In Europe, models predicting the threat of PWD to forest carbon stocks estimated that 1027 Tg C, representing 10% of the continent's total carbon stock, could be at risk from introduced pests, with impacts as severe as current natural disturbances (Seidl et al., 2018). These SDM-based approaches extend beyond static assessments, allowing for more precise predictions of future carbon loss risks and providing robust scientific support for pest management and carbon mitigation strategies. However, existing research lacks a comprehensive multi-dimensional evaluation framework that can predict the interactions between pest outbreaks, the spatial distribution of carbon losses, and forest recovery, particularly in the accurate identification of high-risk areas. Additionally, most studies tend to focus on the short-term effects of PWD, with limited exploration of its long-term ecological impacts and the recovery potential of affected forests.

The aim of this study is to develop a comprehensive model by integrating multi-source data, including remote sensing, forest inventory, and meteorological data, to fully assess the potential impact of PWD infestation on China's forest carbon stocks and predict future carbon loss risks. By combining multi-dimensional data and modeling approaches, this study seeks to overcome the limitations of traditional field observations and single remote sensing techniques, providing more accurate quantification of carbon loss and long-term ecological recovery potential. In this study: (1) Pest occurrence data and climate information are used in the MaxEnt model to generate a pest fitness index; (2) Tree species distribution and vegetation susceptibility are mapped using forest inventory and classification; (3) Lidar remote sensing and root-shoot ratio calculations evaluate aboveground and belowground carbon storage; (4) Regions with live carbon threatened by pests are identified by integrating pest fitness, host distribution, and carbon storage data; (5) The REGIME model estimates carbon recovery time considering live carbon residence time, net primary production, and legacy carbon.

2. Material and methods

2.1. Fitness index of pests

The formulation of a fitness index (FI) for invasive alien pests is essential for discerning their capacity to establish and spread in new environments. This index furnishes insights into the pest's potential for dissemination and its consequent impact on forest ecosystems. The study employed comprehensive pest occurrence data from China for the year 2022 to conduct a detailed analysis of the distribution of PWD. The data for PWD were obtained from the Forest and Grassland Pest Control Station of the State Forestry and Grassland Administration of China (https://www.forestry.gov.cn/). These data were compiled by district and county forestry bureaus and reported biannually through systematic surveys. Additionally, bioclimatic variables for the years 2018–2022 from ERA5-Land (https://www.ecmwf.int/en/era5-land) were used to describe the current climate's temperature and precipitation conditions. The meteorological data from 2018–2022 were selected to smooth out any potential anomalies from single extreme weather years, ensuring more robust species distribution predictions and aligning with the temporal range of the LiDAR data used for carbon stock calculations. These variables include mean diurnal range (bioA, °C), minimum temperature of the coldest month (bioB, °C), mean temperature of the warmest quarter (bioC, °C), and annual precipitation (bioD, m), which define species distribution limits set by extreme temperatures, available energy, and moisture (Hijmans et al., 2005).

Due to the efficacy of MaxEnt software (https://biodiversityinformatics.amnh.org/open_source/maxent/) in processing presence-only data, it was selected to predict the FI of invasive alien pests. The model was parameterized by correlating the species occurrence data for the year 2022 with climate data from 2018–2022, and spatial point autocorrelation was addressed using the SDMtoolbox (http://www.

Table 1
Pine wilt disease host tree susceptibility index (SI) grading.

Type	Family Genus	Species	SI
needle leaved forest	*Pinaceae Pinus*	*P. densiflora, P. thubergii, P.massoniana, P. kesiya var. langbianensis, P. tabuliformis, P.henryi, P. fenzeliana, P.armandii, P. taiwanensis, P. sibirica, P. yunnanensis var. tenuifolia, P. yumnanensis, P. densata, P. palustris, P. wallichiana, P. syvestis var. mongolica, P. pumila, P. syvestis var. mongolica, P. bungeana*	0.9
	Pinaceae Larix	*L. olgensis, L. gmelinii var.principis-rupprechtii, L. kaempferi, L. sibirica, L. gmelinii (Ruprecht), L. olgensis, L. var. macrocarpa, L. potaninii, L. chinensisBeissn*	0.6
	Pinaceae Abies	*A. nephrolepis, A. fargesii, A. delavavi, A. forrestii, A. georgei var. smithii, A. firma, A. firma, A. densa,A. fargesii var. faxoniana, A. delavavi var. motuoensis, A. kawakamii, A. pindrow, A. georgei*	
	Cupressaceae	*J. przewalskii, J. komarovii, Platycladus orientalis, Jmiperusrigida, Cupressus funebris, J. tibetica,Cuninghamia lanceolata, J. saltuaria, J. convallium, J. moirisonicola*	0.3
	Pinaceae Picea	*P.meyeri, P. crassifolia, P. wilsonii, P. obovate, P. schrenkiana, P. schrenkiana, P. jezoensis, P. koraiensis Nakai, P. likiangensis var. rubescens, P. likiangensis,*	
	Pinaceae Tsuga	*P. jezoensis, P. linzhiensis, P. momisonicola, P. brachytyla, P. asperata, P. purpurea T. chinensis, T. formosana, T. dumosa*	
	mixed forest	*P. koraiensis Siebold & Zucc, Chamaecyparis obtusa var. formosana, T. chinensis var. tchekiangensis, A. holophylla*	0.1

sdmtoolbox.org/) for the raw input data. The FI was computed using the formula (Phillips et al., 2006):

$$FI_w(y|x) = \frac{1}{Z_w(x)} \exp\left(\sum_{i=1}^{n} w_i f_i(x,y)\right) \quad (1)$$

$$Z_w(x) = \sum_{y} \exp\left(\sum_{i=1}^{n} w_i f_i(x,y)\right) \quad (2)$$

where x represents each input environmental variable, y is the location of the pests occurrence, $f_i(x,y)$ is the characteristic function, w_i is the weight of the characteristic function, n represents pests occurrence point size, and $FI_w(y|x)$ is the spatial distribution of the FI of pests. The bootstrap method was applied to generate results, with 50 replications for robustness. Pest occurrence data were randomly split: 80% for model training and 20% for testing. The feature classes (FC) used in this study include hinge, product, linear, and quadratic, which were selected after extensive testing to capture the complex relationships between environmental variables and species distribution in a scenario with a large number of presence points. The regularization multiplier (RM) was set to the default value of 1 to balance model complexity and avoid overfitting, based on the optimal performance observed during model testing.

2.2. Distribution of host tree species and division of vegetation resistance

A systematic approach to distinguishing host tree species and their corresponding vegetation resistance indices is critical for the accurate assessment of carbon loss risks due to pest infestations. Our analysis leveraged the extensive arboreal data available in the "Vegetation Map of the People's Republic of China (1:1,000,000)" (Zhang et al., 2007), a comprehensive resource that delineates the distribution of tree species across various forest types in China (https://www.plantplus.cn/dsite/zhibei/b12.html). Utilizing this map, we methodically extracted information relevant to the subcategories of coniferous and mixed forests and classified their resistance to PWD invasion. Host tree species' resistance levels were quantified using a susceptibility index (SI), divided into four categories: extremely susceptible (0.9), high susceptible (0.6), medium susceptible (0.3), and low susceptible (0.1). The SI gradients of 0.1, 0.3, 0.6, and 0.9 reflect the intrinsic resistance levels of trees following pest outbreaks. These values were chosen based on an in-depth classification assessment of tree families and genera, combined with relevant research findings and empirical data from parasitic survival trials. The SI values were calculated as the midpoints of four gradient ranges (0–0.2, 0.2–0.4, 0.4–0.8, and 0.8–1) (Yang et al., 1993; Daub, 2008; Zheng and Khan, 2023). For instance, the 0–0.2 SI range represents mixed forests with coniferous and broadleaf species, which include a substantial proportion of non-host species, and within which coniferous species show strong pest resistance. The 0.2–0.4 SI range corresponds to species with higher resistance, such as those in the families *Cupressaceae* and *Piceaceae Picea*, whereas the most susceptible species, such as *Pinus thunbergii* and *Pinus massoniana*, fall into the highest SI category. These thresholds were established by analyzing survival data from infection trials across different forest types, providing a standardized classification system. While it is challenging to specify the mortality rates for individual tree species in large-scale carbon loss calculations, these SI values represent reasonable average resistance levels within each category, facilitating comprehensive carbon loss assessments and accounting for the statistical significance of tree species groups. Thus, the SI serves as an indicator of potential carbon loss risks, where higher values indicate lower resistance to pest incursions. The exhaustive classification of this SI is available in Table 1.

2.3. Carbon storage of forest trees

Accurate quantification of forest carbon storage is imperative for assessing the carbon loss vulnerability due to pest disturbances. Employing advanced lidar remote sensing technology substantially enhances the efficiency and coverage of carbon stock assessments, providing a broader and more rapid evaluation than is possible with conventional forest inventories. This technological approach facilitates a comprehensive understanding of forest carbon dynamics on a large scale, essential for modeling the impact of pest-induced carbon loss. The aboveground carbon(AGC) storage was quantified utilizing LiDAR remote sensing data from "Global Forest Aboveground Carbon Stocks and Fluxes from GEDI and ICESat −2, 2018-2021" (Ma et al., 2023). The Ecosystem Demography (ED) model (Moorcroft et al., 2001), which encompasses submodules such as growth, decay, hydrology, carbon cycle, and soil biogeochemistry, was employed to simulate and characterize the carbon dynamics within the forests. LiDAR data used in this study were obtained from two NASA missions: GEDI and ICESat −2. GEDI, launched from the International Space Station in December 2018, is a high-resolution laser instrument specifically designed to measure forest vertical structure (Dubayah et al., 2020). ICESat −2, launched in September 2018, aims to measure global surface elevation and vegetation height over land Markus et al. (2017), Neuenschwander and Pitts (2019). To align the data from these two LiDAR missions,

canopy height histograms, average canopy height, and sample density were calculated using the RH100 attribute from GEDI L2 A and the h-canopy attribute from ICESat −2 ATL08. These data were employed for the initialization of the ED model and for assessing the consistency between the two missions' observations. By filtering high-quality LiDAR samples, canopy height histograms at a 0.01° grid scale were further refined into 90 layers, with each layer recording the number of LiDAR samples within a height range of 5 to 50 m, thereby generating high-precision forest structure data layers (https://lpdaac.usgs.gov/). For the computation of underground carbon(UGC) storage, we multiplied the derived AGC storage values by the Root-Shoot Ratio (RSR). The RSR values were sourced from the "Guideline on carbon stock accounting in forest ecosystems" as per the forestry industry standards of the People's Republic of China (https://www.forestry.gov.cn/). The guideline offers a comprehensive set of RSR parameters for various tree species, as detailed in Supplementary Table S1. This methodology ensured a holistic approach to carbon accounting, reflecting both the visible and subterranean carbon reserves of forest trees. Simultaneously, for data visualization, we calculated the latitudinal and longitudinal profiles of forest carbon stocks. The values were obtained by averaging the grid data at the same longitude or latitude after removing outliers, and distinguishing between AGC and UGC stocks.

2.4. Live carbon at risk

To assess the potential loss of live carbon storage in forest ecosystems due to pest invasions, which is integral to the risk evaluation of carbon sequestration, we have formulated an equation:

$$\text{Live C at risk} = FI \times SI \times (AGC + UGC) \tag{3}$$

where FI, ranging from 0 to 1, reflects the adaptability of pest populations under varying climate conditions. Given that PWD is caused by a parasitic pest, we define FI within our formula as the proportion of the host tree population within a region that is affected post-pest invasion. A higher FI indicates a larger fraction of the tree population is affected, signifying a stronger parasitic infestation capability of the pest. Similarly, the SI, ranging from 0 to 1, is employed to quantify the vulnerability of trees to pest infestation and subsequent mortality. In the context of PWD, the SI is approximated to the tree mortality rate, that is, the rate of carbon loss; the greater the SI, the higher the risk of tree mortality and hence the carbon loss rate. AGC, quantified in kilograms of carbon per square meter (Kg C/m^2), represents the carbon stored in forest trees above the soil surface, as derived from lidar remote sensing data. UGC, also measured in Kg C/m^2, reflects the carbon stored in root systems, estimated by combining AGC data with the RSR. The integration of these indices provides a comprehensive measure of the vulnerability of forests to carbon loss. The application of this formula illustrates the potential impact of pest infestations on both aboveground and underground carbon reserves, quantifying the risk to the forest's carbon sequestration capabilities.

2.5. Carbon recovery time

Following a pest invasion, assessing the time required for a forest ecosystem to recover the lost carbon is crucial for forest management decisions and evaluating the forest's resilience to invasive pests. To calculate the carbon recovery time, we utilized the REGIME model (Weng et al., 2012) developed by Weng et al. This model establishes a theoretical framework to quantitatively assess the carbon storage capacity of ecosystems under different disturbance regimes, integrating concepts of carbon influx, carbon pool stability and residence time. It offers a systematic method for understanding the interactions between biogeochemical cycles and disturbance mechanisms. We demonstrate our derivation of the final carbon recovery formula through the REGIME model in the following process, with the first part employing a conceptual biogeochemical cycle (BGC) model that characterizes the ecosystem carbon cycles within litter, biomass, and soil organic matter (SOM) carbon pools:

$$\frac{dX(t)}{dt} = AR^{-1}X(t) + BU(t) \tag{4}$$

where $X(t)$ is ecosystem carbon content at time t; the 3×3 matrix A describes carbon transfer in the three parts. $A = \begin{pmatrix} -1 & 0 & 0 \\ 1 & -1 & 0 \\ 0 & \eta & -1 \end{pmatrix}$ and η is carbon transfer coefficient from the litter pool to the SOM pool. R is a 3×3 diagonal matrix. The diagonal elements, τ_1, τ_2, and τ_3, are the residence times of the carbon in biomass, litter, and SOM, respectively. The vector B represents the allocation coefficients of carbon influx to the three parts, $B = (1 \quad 0 \quad 0)^{\top}$. $U(t)$ denotes the carbon influx at time t.

In the absence of transfers between the litter and soil organic matter pools, a particular solution to the differential equation after a pest disturbance occurs is:

$$X_1 = U\tau_1(1 - e^{-t/\tau_1}) + X_{1,0} \cdot e^{-t/\tau_1} \tag{5}$$

where X_1 is the overall carbon of biomass at time t since last disturbance. For each disturbance cycle, carbon is divided into two units: legacy carbon from the previous circulation and new carbon generated following the disturbance event. The legacy carbon decomposes exponentially $X_{1,\text{old}} = X_{1,0} \cdot e^{-t/\tau_1}$, where $X_{1,0}$ represents the initial amount of legacy carbon immediately after a disturbance outcome; the newly accumulated carbon follows the formula $X_{1,\text{new}} = U\tau_1(1-e^{-t/\tau_1})$. Consequently, we solved for t in the aforementioned formula, yielding the carbon recovery time following pest disturbance:

$$t = -\tau_1 \cdot \ln\left(\frac{f \cdot X_1 - U \cdot \tau_1}{X_{1,0} - U \cdot \tau_1}\right) \tag{6}$$

where f denotes the fraction of the forest's live tree carbon stocks deemed recovered, we assumed complete recuperation when a last pest-infested forest reattains 99% of its existing carbon standard, thus f is set to 0.99. The variable U, representing net primary production (NPP, Kg C/m^2), was determined using data from the MOD17A3HGF V6.1 product for the years 2002–2021 (https://doi.org/10.5067/MODIS/MOD17A3HGF.061), downloaded from Google Earth Engine (GEE). This product provides information about annual gross primary production (GPP) and NPP at a 500 m pixel resolution. Annual NPP is calculated as the sum of all 8-day net photosynthesis (PSN) products (MOD17A2H) from the specified year. X_1 signifies the total carbon, which is computed as the sum of AGC and UGC as calculated previously. $X_{1,0}$ represents the legacy carbon, determined by subtracting the previously calculated Live C at risk from the total carbon. In a forest state of long-term stability, the carbon loss and input maintain a dynamic equilibrium (Pugh et al., 2019). Therefore, we computed the residence time of carbon τ_1, using the following formula:

$$\tau_1 = \frac{\widehat{X_1}}{U} \tag{7}$$

where $\widehat{X_1}$ represents the long-term equilibrium carbon storage of forests. We calculated the carbon storage of Chinese forests over nearly two decades using the dataset "Above-and belowground forest biomass carbon pool in China during 2002-2021" (Chen et al., 2023).

3. Results

3.1. Fitness distribution of PWD

Based on the occurrence points of PWD depicted in Fig. 1(a) and associated climatic variables, we have constructed the spatial distribution of the FI for PWD in China as shown in Fig. 1(b). Our analysis suggests that under current climatic conditions, there is a potential risk of PWD occurrence throughout almost all of China. The Maxent model

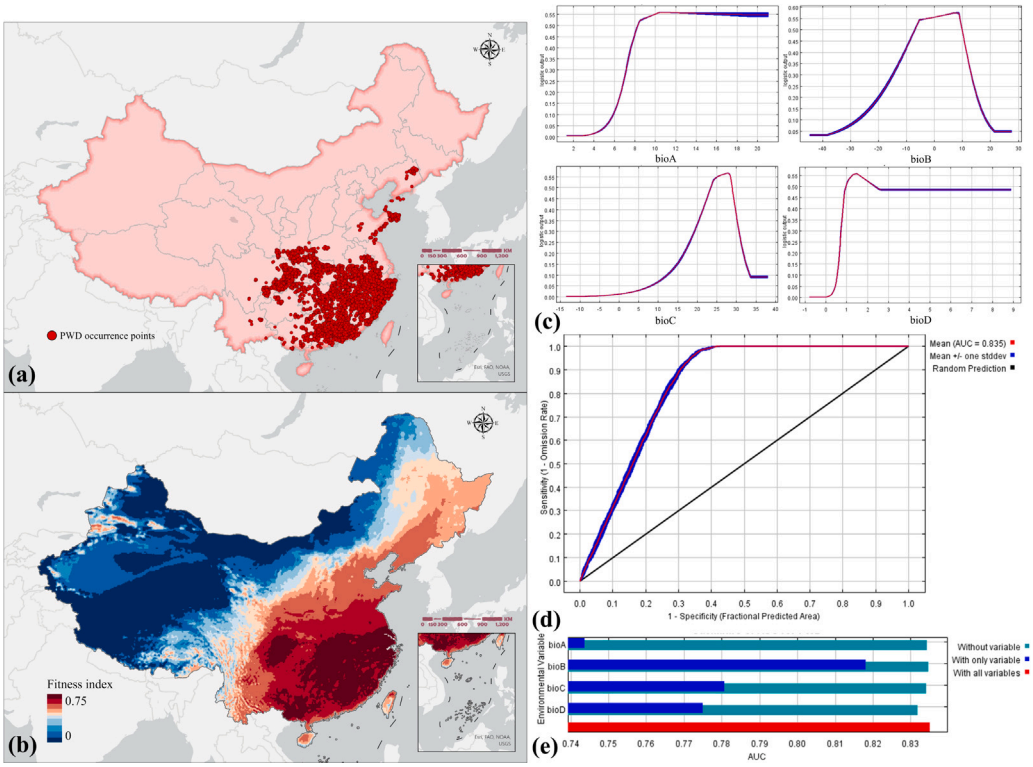

Fig. 1. Distribution of fitness for pine wilt disease (PWD) under the influence of various climatic variables. (a) Occurrence points of PWD. (b) Spatial distribution of the fitness index (FI) for PWD. (c) Partial correlation plots of the PWD's FI with various environmental variables. Each curve is generated by varying the current variable while holding other variables at their average values at presence locations. The *y*-axis displays the predicted FI values derived from the logistic output format, and the *x*-axis represents the original variable values. The curves illustrate the mean reaction from 50 replicate Maxent runs (red) and the mean +/− one standard deviation (blue). (d) Receiver operating characteristic (ROC) curve. The closer the area under the curve (AUC) is to 1, the better the model's predictive capability. (e) Jackknife test. This test evaluates the contribution of each environmental variable to the model's predictive performance. The graph displays the AUC values for each variable used in isolation (blue bars), all other variables excluding the one in question (green bars), and all variables used together (red bars), assisting in identifying the variables that contribute the most to model prediction. (For interpretation of the references to color in this figure legend, the reader is referred to the web version of this article.)

has exhibited commendable predictive accuracy, with an AUC value exceeding 0.8 Fig. 1(d), indicative of the model's high performance in forecasting PWD occurrences. The FI displays a trend of gradual decline from the southeastern coastal regions to the northwestern inland, with a slight resurgence in the Ili River Valley region of the Tianshan Mountains. This suggests that the primary areas suitable for PWD are concentrated in the southeast. Using the partial correlation graphs in Fig. 1(c), we assessed the response of PWD's FI to changes in various environmental variables within the Maxent model. Notably, variables such as the mean diurnal range (bioA) and annual precipitation (bioD) exhibit an initial increase followed by stabilization, indicating that lower diurnal temperature variations and reduced precipitation stress the occurrence of PWD. Temperature variables, namely the minimum temperature of the coldest month (bioB) and the mean temperature of the warmest quarter (bioC), demonstrate that an increase in temperature helps to raise the FI value for PWD. However, when bioB surpasses 8 °C and bioC exceeds 27 °C, the FI begins to decline and is no longer suitable for PWD proliferation. We also applied the Jackknife test to evaluate the relative contributions of each climatic variable to the model, with the results displayed in Fig. 1(e). The environmental variable that contributed the most when used alone was bioB, with a percent contribution of 41.4%, indicating that the minimum temperature of the coldest month contains the most useful information for predicting PWD occurrence. The omission of bioD resulted in the largest decrease in model gain, thus highlighting bioD as the variable containing the most critical moisture information not present in the other variables.

3.2. The spatial distribution of the graded resistance of host tree species and the magnitude of carbon storage

We systematically identified host tree species and replaced the vegetation resistance index with the SI, categorizing the results into four levels as shown in Fig. 2. The low susceptible vegetation (0.1) is the least distributed Fig. 2(a), with the main constituents under the mixed forest category being *P. koraiensis Siebold & Zucc, A. holophylla, Chamaecyparis obtusa var. formosana,* and *T. chinensis var. tchekiangensis*. The most widely distributed middle susceptible vegetation (0.3) areas Fig. 2(b), composed of *Cupressaceae, Pinaceae Picea*, and *Pinaceae Tsuga*, are predominantly located in the southern part of China, forming extensive breeding grounds. The northeastern Greater Khingan Range, southern coastal areas, and southwestern mountainous regions of China are the distribution areas for high susceptible vegetation (0.6) Fig. 2(c), with the primary Family Genus being *Pinaceae Larix* and *Pinaceae Abies*. Scattered throughout Fig. 2(d) are areas of extremely susceptible vegetation (0.9), mainly consisting of low resistance species under *Pinaceae Pinus* such as *P. densiflora, P. thubergii, P. massoniana*, and others.

Fig. 3's main map and the longitudinal and latitudinal profiles located at the top and left depict the distribution of carbon storage within host tree species across China, reaching up to 28.17 kgC/m^2. In the profiles, green represents the carbon storage of aboveground live host trees, while brown denotes that of underground live host trees, quantifying the carbon content along different geographical axes. The latitudinal profile exhibits significant peaks at the northern and southern ends, with aboveground carbon storage exceeding 6 kgC/m^2 in

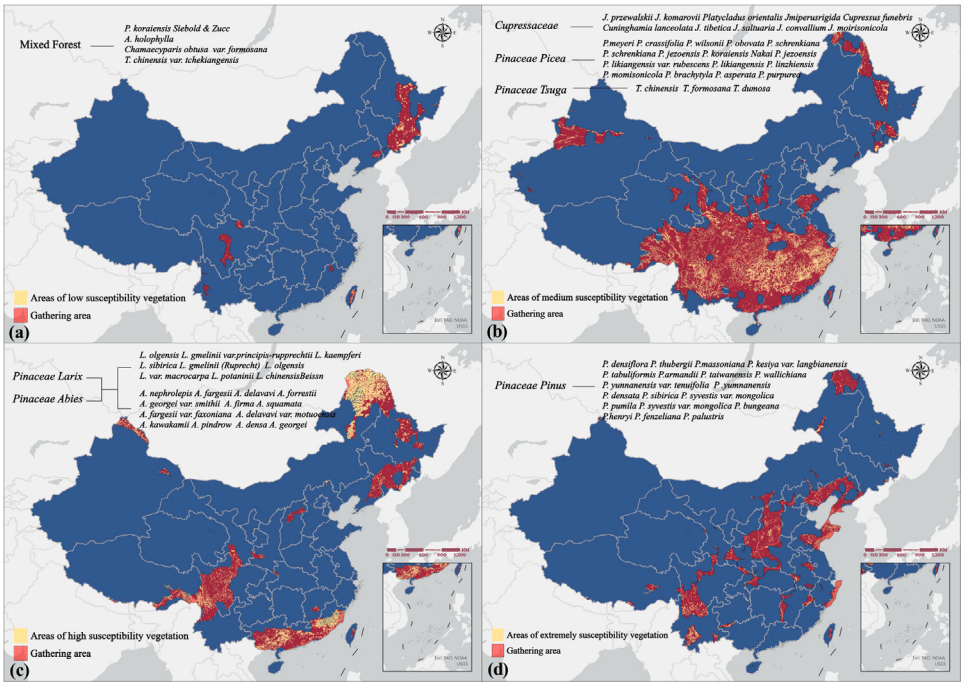

Fig. 2. Distribution of host tree species and division of vegetation resistance. The yellow areas in the figure represent the specific growth regions of vegetation with different species resistances, and the red areas denote their gathering growth zones. Susceptibility index (SI): (a) low susceptible, 0.1; (b) medium susceptible, 0.3; (c) high susceptible, 0.6; (d) extremely susceptible, 0.9. (For interpretation of the references to color in this figure legend, the reader is referred to the web version of this article.)

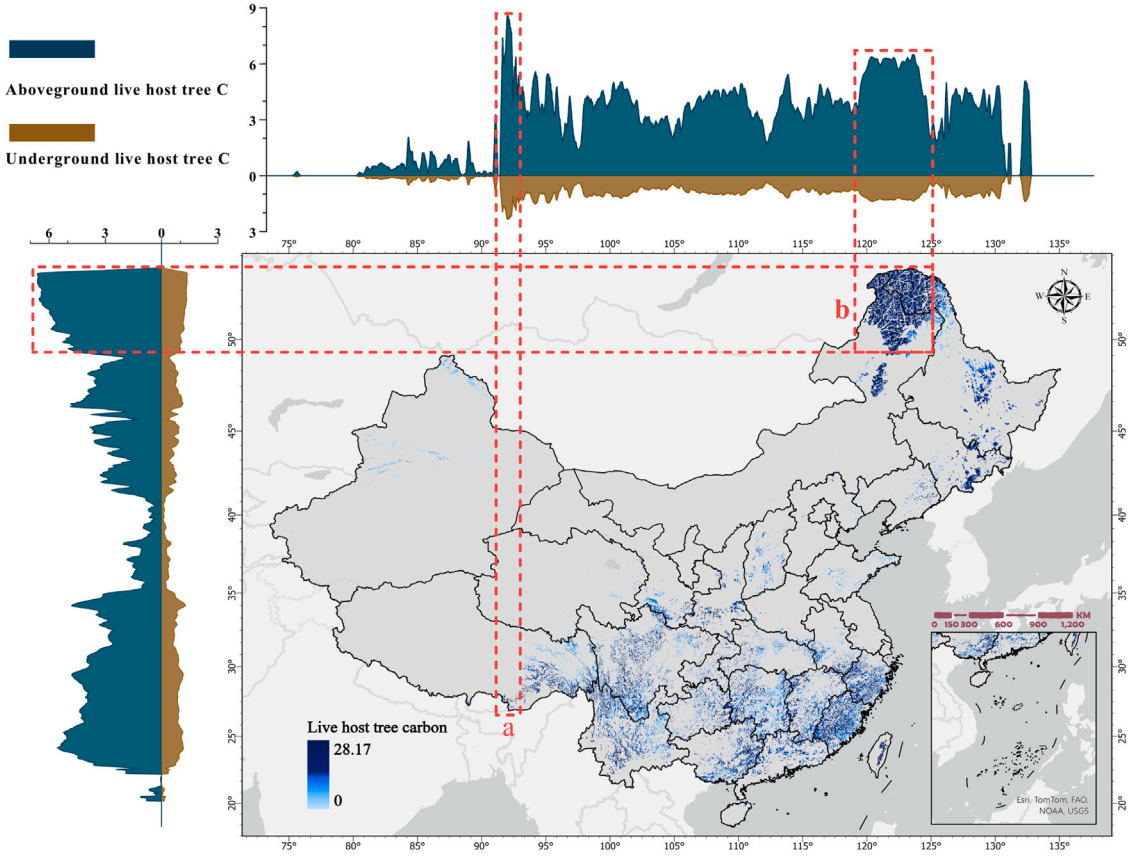

Fig. 3. Carbon storage of live host trees (Kg C/m^2). The subfigures at the top and left of the map are longitudinal and latitudinal profiles of the carbon storage of host tree species, calculated based on average values, with green and brown representing the carbon content of the aboveground and underground parts, respectively. The red boxes marked as a and b indicate areas of high carbon storage that are the focus of attention. (For interpretation of the references to color in this figure legend, the reader is referred to the web version of this article.)

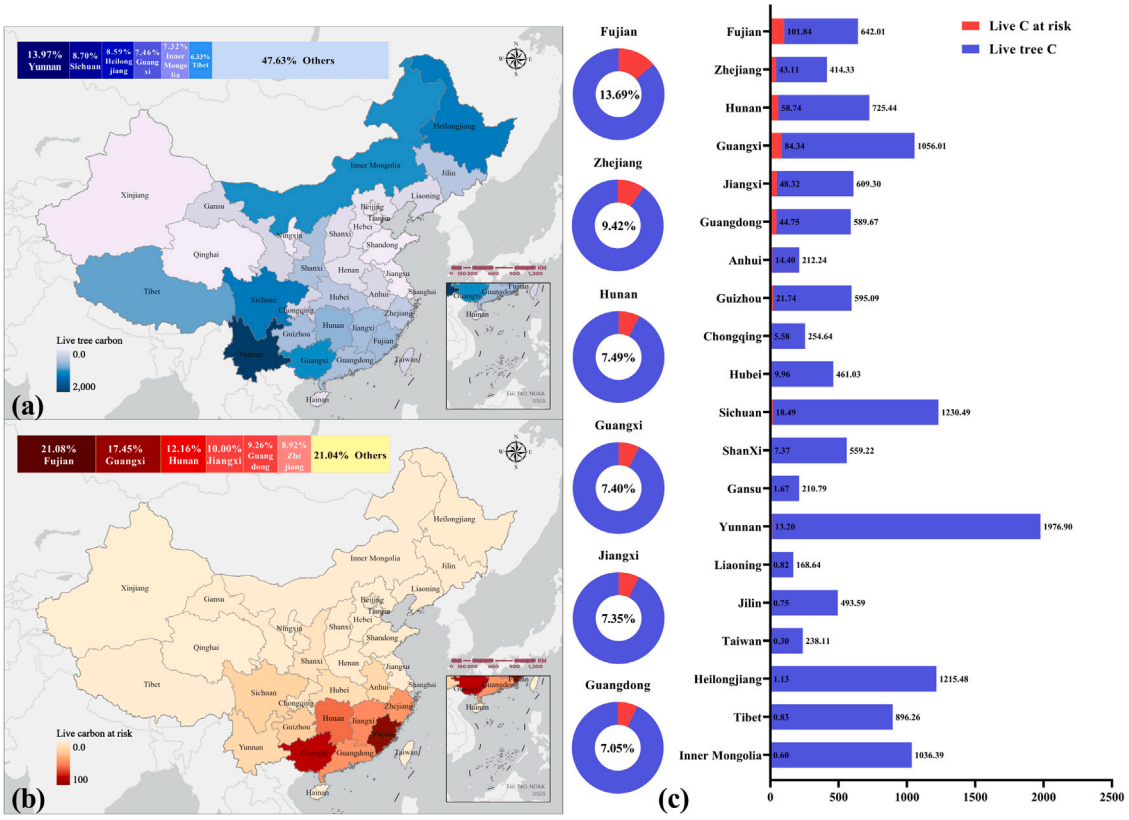

Fig. 4. The provincial delineation of live carbon risk patterns. (a) The bar chart above displays the top six provinces in terms of the proportion of total live tree carbon (Tg C) within each provincial region, the same below. (b) The provincial distribution of all live carbon at risk (Tg C). (c) The arrangement of the proportion of risk carbon. Red and blue represent the risk carbon and total tree carbon, respectively, and the left circular chart shows the top six provinces in terms of the proportion of risk in the right columnar carbon storage (Tg C). (For interpretation of the references to color in this figure legend, the reader is referred to the web version of this article.)

peak regions, indicating these areas as major contributors to the forest's overall carbon budget. The longitudinal profile reveals an uneven distribution of carbon, with host tree species in the eastern regions showing a scarcity of carbon storage, whereas substantial carbon storage is present at specific longitudes. Particularly, the red dashed boxes marked 'a' in the Himalayan valleys and 'b' in the Greater and Lesser Khingan Ranges of the northeast represent areas of high carbon storage, with the 'a' region having an average total carbon storage in host tree species exceeding 11 kgC/m^2. Understanding the distribution of carbon within forest ecosystems is heavily dependent on these regions, pinpointing potential hotspots for carbon sequestration.

3.3. The regional pattern of at-risk live carbon in host tree species

To elucidate the risk posed to the existing live carbon in trees by PWD invasion, we first tallied the live tree carbon storage in forests across all provinces of China Fig. 4(a). The total live tree carbon storage in Chinese forests amounts to 14,151.04 Tg C, with Yunnan having the highest at 1,976.9 Tg C, accounting for 13.97% of the total; followed by Sichuan with 1,230.49 Tg C (8.7%), Heilongjiang with 1,215.48 Tg C (8.59%), Guangxi with 1,056.01 Tg C (7.46%), Inner Mongolia with 1,036.39 Tg C (7.32%), and Tibet with 896.26 Tg C (6.33%). Overall, there is a concentration of high-value carbon storage in the northeast and southwest, with a scarcity in the central and northwest regions. In Fig. 4(b), we calculated the live carbon at risk in each province following a comprehensive invasion by PWD. The total at-risk carbon in Chinese forests under PWD invasion amounts to 483.23 Tg C, with Fujian having the highest risk live carbon content at 101.84 Tg C, which constitutes 21.08% of the total; followed by Guangxi at 84.34 Tg C (17.45%), Hunan at 58.74 Tg C (12.16%), Jiangxi at 48.32 Tg C (10%), Guangdong at 44.75 Tg C (9.26%), and Zhejiang at 43.11 Tg C (8.92%). The main risk areas for live carbon are primarily concentrated in the southern coastal regions of China and the adjacent provinces, presenting a risk spillover pattern spreading from key areas. We are also concerned with the proportion of carbon at risk relative to the total carbon in the region to measure the level of risk in different areas. It is estimated that with PWD invasion alone, 3.41% of live carbon in Chinese forests will be threatened. Fig. 4(c) displays the six provinces with the highest degree of risk, with Fujian at the top with 13.69%, followed by Zhejiang (9.42%), Hunan (7.49%), Guangxi (7.40%), Jiangxi (7.35%), and Guangdong (7.05%).

In Fig. 4(b), we outline the total at-risk carbon storage for each province in China, and clarifying the specific high-risk areas for carbon loss can aid in precision risk management and governance by administrators in advance. Fig. 5 presents the key changes and hotspots of at-risk live carbon in Chinese forests following a PWD invasion, within the distribution range of host tree species. The main high-risk areas include: (1) the Liangguang Hills in southeastern Guangxi and central Guangdong shown in Fig. 5(c) and (d), respectively. (2) The Zhe-Min Hills located in central Fujian and southern Zhejiang as shown in Fig. 5(f) and (g). (3) The western mountainous area of Hunan and the Jiangnan Hills at the junction of Hunan and Jiangxi depicted in Fig. 5(e). Apart from these southeastern high-risk provinces, other areas show a lower risk of carbon loss due to PWD invasion. It is particularly noteworthy that the Greater and Lesser Khingan Ranges in the northeast, the Yunnan–Guizhou Plateau depicted in Fig. 5(a) and (b), as well as the Hengduan Mountains and Sichuan Plateau above, although being concentrated areas for host tree species and rich in forest carbon storage, are low-risk areas for carbon loss due to PWD invasion.

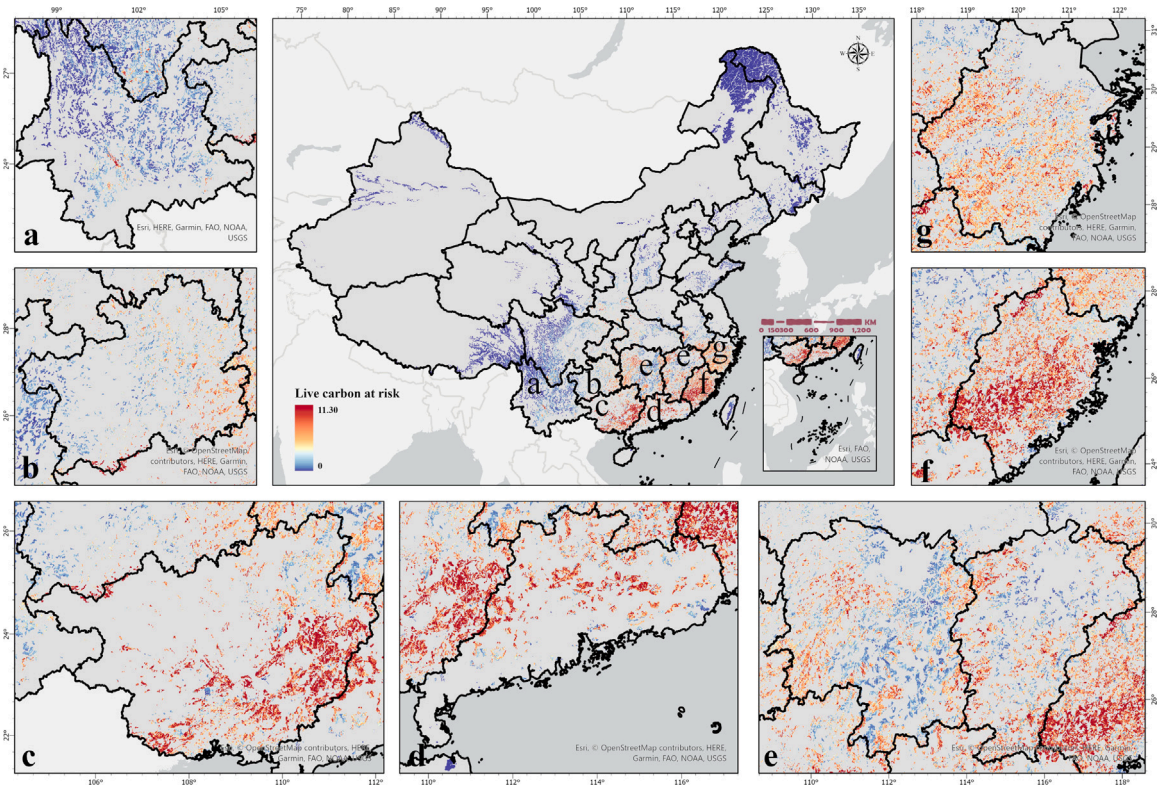

Fig. 5. Focus map of key areas with at-risk live carbon (Kg C/m^2): (a) Yunnan, (b) Guizhou, (c) Guangxi, (d) Guangdong, (e) Hunan, Jiangxi, (f) Fujian, (g) Zhejiang. (For interpretation of the references to color in this figure legend, the reader is referred to the web version of this article.)

3.4. C recovery time

Fig. 6(a) illustrates the recovery time for carbon at risk in Chinese forests following a comprehensive invasion by PWD, ranging from less than a year to several decades, with an average recovery time of 13.95 years. The southeastern hills (SE) exhibit the longest carbon recovery time, averaging 20.03 years, as this region is a major area for PWD propagation and spread Fig. 1(b). The pest finds suitable living conditions here, leading to severe risk carbon loss Fig. 4(b). Therefore, despite maintaining a high level of NPP carbon input Fig. 6(b), the SE region requires the longest time to recover. Moreover, the residence time of carbon and the equilibrium carbon storage also influence the recovery of forest carbon losses. The average recovery times for forests in the northern (NE) and southwestern high-altitude mountain (SW) regions are 14.07 and 10.93 years, respectively. As shown in Fig. 4(b), the SW region exhibits a higher degree of carbon loss risk than the NE region, yet its average carbon recovery time is shorter. This is primarily due to the longer average residence time of live carbon in the NE region Fig. 6(c), where trees grow slowly, and the ecosystem accumulates nutrients at a lower rate than in the SW region. Additionally, the SW region possesses a higher equilibrium carbon storage Fig. 6(d), making forest ecosystems more resistant to invasive pests than those in the NE region. These factors affect the forest carbon risk recovery times in different regions of China.

4. Discussion

China boasts abundant forest resources, among which coniferous forest systems dominated by pine trees play a significant part (Ni, 2003). Over the past decades, China's forest systems have performed a carbon sink function by absorbing carbon dioxide and converting it into biomass, thereby playing a crucial role in climate improvement and regulation (Yao et al., 2018; Magney et al., 2019). However, the carbon sequestration capacity of forests can fluctuate due to invasions by exotic pests or frequent natural disasters (Fang et al., 2018; Fernández-Martínez et al., 2023), especially as the climate-suitable range for pests increases with climate change. Invasions of this nature could significantly amplify climate change by altering forest demographic structures and reducing carbon levels in the biosphere (Körner, 2017). Therefore, predicting forest pest risks and assessing carbon loss recovery is of great importance. To evaluate the recovery from losses caused by invasive PWD at a continental scale, we utilized the REGIME model (Weng et al., 2012) with a simplified derivation. This model, utilizing mathematical descriptions of recovery patterns and disturbance mechanisms, reveals long-term and large-scale carbon dynamics by explaining the interaction between deterministic carbon processes in ecosystems and random disturbance events. However, to obtain meaningful analytical solutions using this model, we highly simplified the complex system of carbon cycle and disturbance occurrence interactions through two assumptions: (1) disturbances do not affect NPP (Net Primary Production) and carbon residence time, (2) the proportion of carbon removed by disturbance events is unrelated to the current biomass carbon content, and (3) the exponential distribution of disturbance intervals. This increases the uncertainty in assessing carbon loss recovery due to pest invasions. In future research, we should expand application scenarios, particularly by developing model parameters for various pest scenarios, to calculate their individual impacts rather than considering all factors collectively (Zhao et al., 2023).

In recent decades, PWD has inflicted extensive damage on China's forests, resulting in the loss of billions of pine trees and causing significant economic and ecological harm. The direct economic loss and the value of lost ecosystem services are estimated to be up to $250 million, making this issue one of the most dangerous and destructive diseases in forest ecosystems globally (Zhao et al., 2023). Given the present climate conditions, our research indicates that the comprehensive invasion of PWD into China's forests could lead to potential carbon losses up to 483.23 Tg C. This implies that the affected forests are transitioning from carbon sinks to carbon sources, with the carbon loss attributed to PWD

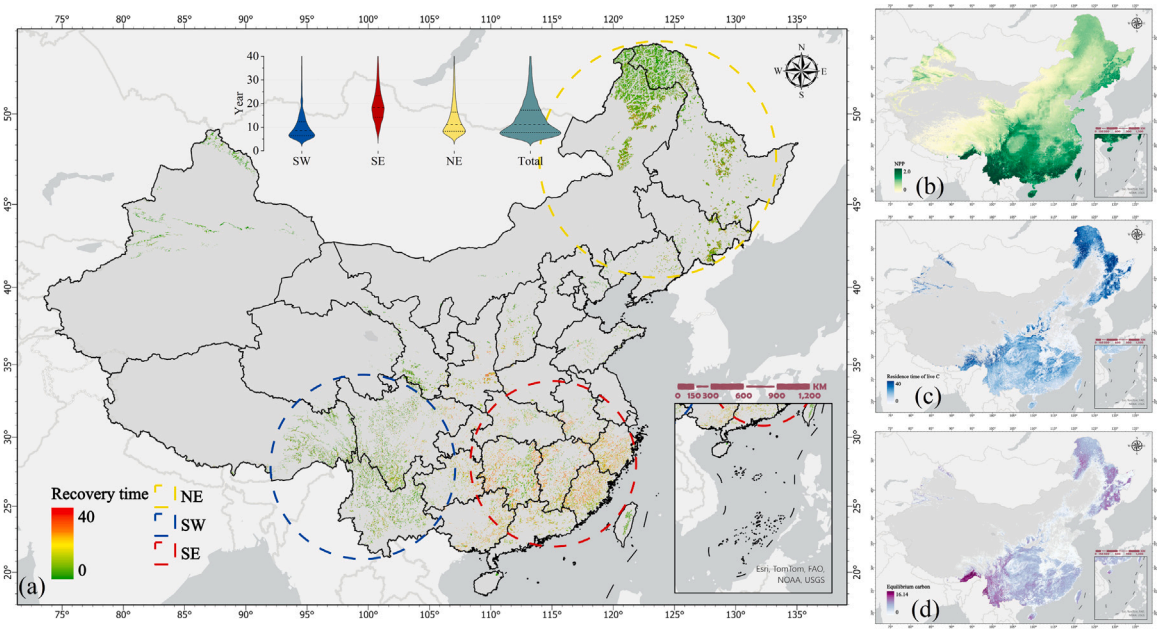

Fig. 6. Potential recovery from live tree carbon loss caused by pine wilt disease (PWD) invasion. (a) Carbon recovery time (years). The yellow, blue, and red areas in NE, SW, and SE correspond to the carbon recovery times in the violin plots of the same colors, with the three dashed lines on the violin plot representing the 25th percentile, median, and 75th percentile from bottom to top. For clarity, values greater than 40 years have been truncated. (b) Average net primary production (NPP) from 2002–2021 (Kg C/m^2). (c) Residence time of live carbon (years). (d) Equilibrium carbon storage from 2002–2021 (Kg C/m^2). (For interpretation of the references to color in this figure legend, the reader is referred to the web version of this article.)

alone equivalent to the carbon dioxide emissions from burning 700,000 tons of standard coal (Adler et al., 2022), posing a serious challenge to China's goals of reaching carbon peak and carbon neutrality. Therefore, effective management and blocking the spread of invasive pests are urgent priorities. For PWD, we recommend adopting a series of proactive management measures, including but not limited to thinning and legal burning, to reduce its spread (Klapwijk et al., 2016). Additionally, we should focus on controlling tree density and strive to create more diversified stand structures to increase biodiversity at different scales, thereby reducing resource competition among trees and enhancing their resistance and recovery capabilities against PWD (Isbell et al., 2017; Diana et al., 2014). These measures not only help mitigate the impact of Pine Wilt Disease on China's forests but also promote the recovery and sustainable development of forest ecosystems, laying a solid foundation for future ecological security and sustainable resource use.

5. Conclusions

Our results demonstrate that by integrating multiple data sources including forest surveys, remote sensing, and meteorological observations, and through a detailed classification of host pine tree resistance across China, the use of the MaxEnt model, a live carbon risk model, and a C recovery REGIME model that incorporates disturbance mechanisms, we can ascertain how forest C risk losses are distributed under PWD invasion, as well as how C recovery in affected forests progresses. We found that the primary risk areas for PWD are concentrated along the southern coast of China and adjacent provinces, exhibiting a risk spillover pattern that radiates from focal areas. The recovery time for risk C varies from less than a year to several decades, with an average recovery time of 13.95 years. The C recovery time is longest in the Southeastern hill regions, averaging 20.03 years, while the average recovery times for northern forests and southwestern high-altitude mountain areas are 14.07 and 10.93 years, respectively. Our framework process considers the multifaceted impacts of PWD on forest carbon storage and provides new insights into the geographic distribution of efforts to mitigate its establishment and spread. This is of significant importance for promoting the recovery of forest ecosystems, maintaining ecological security, and achieving sustainable resource utilization, offering valuable references for future forest ecosystem management and conservation efforts.

CRediT authorship contribution statement

Bohai Hu: Writing – original draft, Methodology, Conceptualization. **Wenjiang Huang:** Writing – review & editing, Software, Investigation. **Zhuoqing Hao:** Writing – review & editing, Methodology. **Jing Guo:** Writing – review & editing. **Yanru Huang:** Writing – review & editing. **Xiangzhe Cheng:** Validation. **Jing Zhao:** Validation. **Quanjun Jiao:** Writing – review & editing. **Biyao Zhang:** Writing – review & editing.

Consent for publication

Not applicable.

Ethics approval and consent to participate

Not applicable.

Funding

This study was supported by the National Key R and D Program of China (2021YFD1400902), National Natural Science Foundation of China (42201355), Technical Support Project for Malaria Control-Elimination in Sao Tome and Principe (3rd Round) (A2-6199-21-411-001), CAS-CNR Project: Research on Remote Sensing Monitoring of Crop Growth and Disease and Pest under the Background of Climate Change.

Declaration of competing interest

The authors declare that they have no known competing financial interests or personal relationships that could have appeared to influence the work reported in this paper.

Appendix A. Supplementary data

Supplementary material related to this article can be found online at https://doi.org/10.1016/j.ecolind.2024.112819.

Data availability

Data will be made available on request.

References

Adler, C., Wester, P., Bhatt, I., Huggel, C., Insarov, G., Morecroft, M., Muccione, V., Prakash, A., 2022. Cross-Chapter Paper 5: Mountains. Cambridge University Press, Cambridge, UK and New York, pp. 2273–2318. http://dx.doi.org/10.1017/9781009325844.022.2273.

lM Arnold, A., Grüning, M., Simon, J., Reinhardt, A.B., Lamersdorf, N., Thies, C., 2016. Forest defoliator pests alter carbon and nitrogen cycles. Royal Soc. Open Sci. 3, 160361.

Bright, B.C., Hicke, J.A., Hudak, A.T., 2012. Estimating aboveground carbon stocks of a forest affected by mountain pine beetle in idaho using lidar and multispectral imagery. Remote Sens. Environ. 124, 270–281.

Brown, M., Black, T., Nesic, Z., Foord, V., Spittlehouse, D., Fredeen, A., Grant, N., Burton, P., Trofymow, J., 2010. Impact of mountain pine beetle on the net ecosystem production of lodgepole pine stands in British Columbia. Agricult. Forest. Meterol. 150, 254–264.

Bustamante, M.M., Roitman, I., Aide, T.M., Alencar, A., Anderson, L.O., Aragão, L., Asner, G.P., Barlow, J., Berenguer, E., Chambers, J., et al., 2016. Toward an integrated monitoring framework to assess the effects of tropical forest degradation and recovery on carbon stocks and biodiversity. Global Change Biol 22, 92–109.

Chen, Y., Feng, X., Fu, B., Ma, H., Zohner, C., Crowther, T., Huang, Y., Wu, X., Wei, F., 2023. Above-and belowground forest biomass carbon pool in China during 20022021. Natl. Tibet. Plateau Data Cent 15, 897–910.

Collalti, A., Tjoelker, M.G., Hoch, G., Mäkelä, A., Guidolotti, G., Heskel, M., Petit, G., Ryan, M.G., Battipaglia, G., Matteucci, G., et al., 2020. Plant respiration: controlled by photosynthesis or biomass? Global Change Biol. 26, 1739–1753.

Daub, M., 2008. Investigations on Pathogenicity, Invasion Biology and Population Dynamics of the Pine Wood Nematode Bursaphelenchus Xylophilus (Steiner Und Buhrer 1934) Nickle 1970 in European Conifers. (Ph.D. thesis). Universitäts-und Landesbibliothek Bonn.

Diana, S., Eric, B., Elisabeth, L., 2014. Management for mountain pine beetle outbreak suppression: Does relevant science support current policy? Forests 5, 103–133.

Dubayah, R., Blair, J.B., Goetz, S., Fatoyinbo, L., Hansen, M., Healey, S., Hofton, M., Hurtt, G., Kellner, J., Luthcke, S., et al., 2020. The global ecosystem dynamics investigation: High-resolution laser ranging of the earth's forests and topography. Sci. Remote Sens. 1, 100002.

Edburg, S.L., Hicke, J.A., Lawrence, D.M., Thornton, P.E., 2011. Simulating coupled carbon and nitrogen dynamics following mountain pine beetle outbreaks in the Western United States. J. Geophys. Res. Biogeosci. 116.

Fang, J., Yu, G., Liu, L., Hu, S., Chapin, III, F.S., 2018. Climate change, human impacts, and carbon sequestration in China. Proc. Natl. Acad. Sci. 115, 4015–4020.

Fernández-Martínez, M., Peñuelas, J., Chevallier, F., Ciais, P., Obersteiner, M., Rödenbeck, C., Sardans, J., Vicca, S., Yang, H., Sitch, S., et al., 2023. Diagnosing destabilization risk in global land carbon sinks. Nature 615, 848–853.

Foster, J., 2011. Forest Insect Defoliation Patterns and Carbon Dynamics: Linking Remote Sensing with Simulation Modeling. (Ph.D. thesis). University of Wisconsin-Madison.

Gao, R., Luo, Y., Wang, Z., Yu, H., Shi, J., 2018. Patterns of biomass, carbon, and nitrogen storage distribution dynamics after the invasion of pine forests by bursaphelenchus xylophilus (nematoda: Aphelenchoididae) in the three gorges reservoir region. J. For. Res. 29, 459–470.

Goetz, S., Dubayah, R., 2011. Advances in remote sensing technology and implications for measuring and monitoring forest carbon stocks and change. Carbon Manag. 2, 231–244.

Hijmans, R.J., Cameron, S.E., Parra, J.L., Jones, P.G., Jarvis, A., 2005. Very high resolution interpolated climate surfaces for global land areas. Int. J. Climatol. 25, 1965–1978.

Hunt, S.L., Newman, J., Otis, G.W., 2006. Threats and Impacts of Exotic Pests under Climate Change: Implications for Canada's Forest Ecosystems and Carbon Stocks. BIOCAP Canada Foundation.

Isbell, F., Gonzalez, A., Loreau, M., Cowles, J., Díaz, S.M., Hector, A., Mace, G.M., Wardle, D.A., O'Connor, M.I., Duffy, J.E., 2017. Linking the Influence and Dependence of People on Biodiversity Across Scales. Nature Publishing Group.

Ji, Y., Zhou, G., Luo, T., Dan, Y., Zhou, L., Lv, X., 2020. Variation of net primary productivity and its drivers in China's forests during 2000–2018. For. Ecosyst. 7, 1–11.

Klapwijk, M.J., Bylund, H., Schroeder, M., Bjrkman, C., 2016. Forest management and natural biocontrol of insect pests. Forestry 89.

Körner, C., 2017. A matter of tree longevity. Science 355, 130–131.

Kurz, W.A., Dymond, C., Stinson, G., Rampley, G., Neilson, E., Carroll, A., Ebata, T., Safranyik, L., 2008. Mountain pine beetle and forest carbon feedback to climate change. Nature 452, 987–990.

Liu, S., Bond-Lamberty, B., Hicke, J.A., Vargas, R., Zhao, S., Chen, J., Edburg, S.L., Hu, Y., Liu, J., McGuire, A.D., et al., 2011. Simulating the impacts of disturbances on forest carbon cycling in North America: processes, data, models, and challenges. J. Geophys. Res. Biogeosci. 116.

Liu, J., He, C., Tang, Y., Liu, W., Xu, Y., Li, Z., Qin, X., Jin, S., 2021. A review of cremastra appendiculata (d. don) makino as a traditional herbal medicine and its main components. J Ethnopharmacol. 279, 114357.

Ma, L., Hurtt, G., Tang, H., Lamb, R., Lister, A., Chini, L., Dubayah, R., Armston, J., Campbell, E., Duncanson, L., Healey, S., O'Neil-Dunne, J., Ott, L., Poulter, B., Shen, Q., 2023. Global forest aboveground carbon stocks and fluxes from gedi and icesat-2. pp. 2018–2021. http://dx.doi.org/10.3334/ORNLDAAC/2180.

Magney, T.S., Bowling, D.R., Logan, B.A., Grossmann, K., Stutz, J., Blanken, P.D., Burns, S.P., Cheng, R., Garcia, M.A., Kohler, P., et al., 2019. Mechanistic evidence for tracking the seasonality of photosynthesis with solar-induced fluorescence. Proc. Natl. Acad. Sci 116, 11640–11645.

Mamiya, Y., 1983. Pathology of the pine wilt disease caused by bursaphelenchus xylophilus. Annu. Rev. Phytopathol. 21, 201–220.

Markus, T., Neumann, T., Martino, A., Abdalati, W., Brunt, K., Csatho, B., Farrell, S., Fricker, H., Gardner, A., Harding, D., et al., 2017. The ice, cloud, and land elevation satellite-2 (icesat-2): science requirements, concept, and implementation. Remote Sens. Environ. 190, 260–273.

Mitchell, R.G., Preisler, H.K., 1998. Fall rate of lodgepole pine killed by the mountain pine beetle in central oregon. West. J. Appl. For. 13, 23–26.

Moorcroft, P.R., Hurtt, G.C., Pacala, S.W., 2001. A method for scaling vegetation dynamics: the ecosystem demography model (ed). Ecol. Monograph 71, 557–586.

Neuenschwander, A., Pitts, K., 2019. The atl08 land and vegetation product for the icesat-2 mission. Remote Sens. Environ. 221, 247–259.

Ni, J., 2003. Net primary productivity in forests of china: scaling-up of national inventory data and comparison with model predictions. Forest Ecol. Manag. 176, 485–495.

Nunes, L.J., Meireles, C.I., Pinto Gomes, C.J., Almeida Ribeiro, N.M., 2020. Forest contribution to climate change mitigation: Management oriented to carbon capture and storage. Climate 8 (21).

Pfeifer, E.M., Hicke, J.A., Meddens, A.J., 2011. Observations and modeling of aboveground tree carbon stocks and fluxes following a bark beetle outbreak in the western united states. Global Change Biol. 17, 339–350.

Phillips, S.J., Anderson, R.P., Schapire, R.E., 2006. Maximum entropy modeling of species geographic distributions. Ecol. Model. 190, 231–259.

Pugh, T.A., Arneth, A., Kautz, M., Poulter, B., Smith, B., 2019. Important role of forest disturbances in the global biomass turnover and carbon sinks. Nat. Geosci. 12, 730–735.

Quirion, B.R., Domke, G.M., Walters, B.F., Lovett, G.M., Fargione, J.E., Greenwood, L., Serbesoff-King, K., Randall, J.M., Fei, S., 2021. Insect and disease disturbances correlate with reduced carbon sequestration in forests of the contiguous united states. Front. For. Glob. Chang. 4, 716582.

Seidl, R., Klonner, G., Rammer, W., Essl, F., Moreno, A., Neumann, M., Dullinger, S., 2018. Invasive alien pests threaten the carbon stored in Europe's forests. Nat. Commun 9 (1626).

Shaikh, T.A., Rasool, T., Lone, F.R., 2022. Towards leveraging the role of machine learning and artificial intelligence in precision agriculture and smart farming. Comput. Electron. Agric. 198, 107119.

Thom, D., Rammer, W., Seidl, R., 2017. The impact of future forest dynamics on climate: interactive effects of changing vegetation and disturbance regimes. Ecol. Monographs 87, 665–684.

Valley, F.O.D., 2014. Impact of infestation of sal heartwood borer (hoplocerambyx spinicornis) on the carbon stock of sal (shorea robusta).

Wang, W., Peng, W., Liu, X., He, G., Cai, Y., 2022. Spatiotemporal dynamics and factors driving the distributions of pine wilt disease-damaged forests in China. Forests 13 (261).

Wang, W., Zhu, Q., He, G., Liu, X., Peng, W., Cai, Y., 2023. Impacts of climate change on pine wilt disease outbreaks and associated carbon stock losses. Agricult. Forest. Meterol. 334, 109426.

Weng, E., Luo, Y., Wang, W., Wang, H., Hayes, D.J., McGuire, A.D., Hastings, A., Schimel, D.S., 2012. Ecosystem carbon storage capacity as affected by disturbance regimes: A general theoretical model. J. Geophys. Res. Biogeosci..

Yang, B., Hu, K., Wang, Q., Sun, Y., Wu, Z., Wang, Q., 1993. Studies on the resistance of pine trees to pine wood nematode, bursaphelenchus xylophilus. J. For. Res. 6, 249.

Yao, Y., Piao, S., Wang, T., 2018. Future biomass carbon sequestration capacity of Chinese forests. Sci. Bull. 63, 1108–1117.

Yuan, H.S., Wei, Y.L., Wang, X.G., 2015. Maxent modeling for predicting the potential distribution of Sanghuang, an important group of medicinal fungi in China. Fungal Ecol. 17, 140–145.

Zhang, X., Sun, S., Yong, S., Zhou, Z., Wang, R., 2007. Vegetation map of the People's Republic of China (1: 1000000). Geol. Publ. House.

Zhang, D., Zuo, X., Zang, C., 2021. Assessment of future potential carbon sequestration and water consumption in the construction area of the three-north shelterbelt programme in China. Agricult. Forest. Meterol. 303, 108377.

Zhao, H., Xian, X., Yang, N., Guo, J., Zhao, L., Shi, J., Liu, 2023. Risk assessment framework for pine wilt disease: Estimating the introduction pathways and multi-species interactions among the pine wood nematode, its insect vectors, and hosts in China. Sci. Total Environ. 905, 167075.

Zheng, Y., Khan, M.R., 2023. Pine wood nematode in coniferous forests and their management by novel biological and biotechnological interventions. In: Novel Biological and Biotechnological Applications in Plant Nematode Management. Springer, pp. 489–514.